

A ferroptosis-inducing iridium(III) complex

Xiuxiu Wang^{1,2†}, Feng Chen^{2†}, Jingyi Zhang², Jianxuan Sun², Xinyang Zhao², Yuelu Zhu²,
Wei Wei^{1*}, Jing Zhao^{1,2*} & Zijian Guo^{2*}

¹State Key Laboratory of Coordination Chemistry, Institute of Chemistry and Biomedical Sciences, School of Life Sciences, Nanjing University, Nanjing 210023, China;

²School of Chemistry and Chemical Engineering, Nanjing University, Nanjing 210093, China

Received June 27, 2019; accepted August 5, 2019; published online September 17, 2019

Ferroptosis is a recently emerging non-apoptotic mode of cell death involving the production of iron-dependent reactive oxygen species (ROS). Here we described a mitochondria-targeted iridium (III) complex IrFN that exhibited potent antiproliferative activity against a variety of cancer cells, especially the A2780 human ovarian cancer cells, through the ferroptosis pathways. Mechanistic studies by label-free quantitative proteomics profiling indicated that heme oxygenase 1 (HMOX1)-mediated ferroptosis process was activated by IrFN. The study on iron-dependent cell death, ROS accumulation, lipid peroxidation, and over released iron further confirmed the ferroptosis processes. mRNA transcription quantification, *in vitro* over-expression of HMOX1, and RNAi-mediated knock-down experiments suggested that IrFN activated the over-expression of HMOX1. Our report revealed the first case of anticancer iridium complex leading to ferroptosis, highlighting ferroptosis as a promising approach in future design of metallodrugs.

iridium, proteome, ferroptosis, heme oxygenase 1

Citation: Wang X, Chen F, Zhang J, Sun J, Zhao X, Zhu Y, Wei W, Zhao J, Guo Z. A ferroptosis-inducing iridium(III) complex. *Sci China Chem*, 2020, 63: 65–72. <https://doi.org/10.1007/s11426-019-9577-3>

1 Introduction

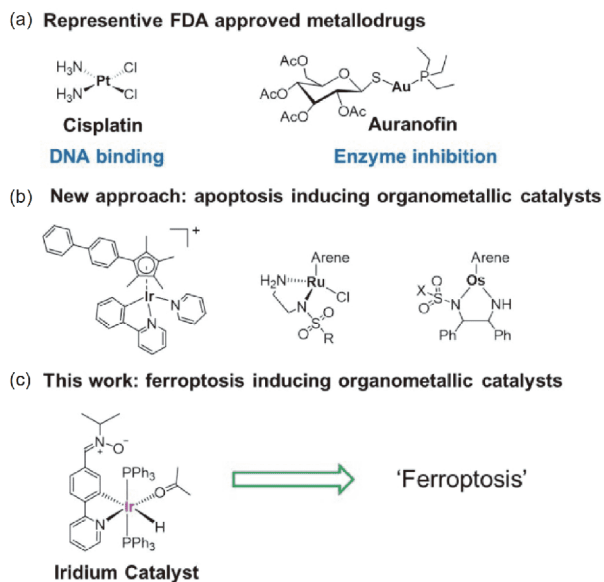
Transition metal complexes have been a rich source of anticancer drug candidates since the landmark discovery of cisplatin [1]. The proposed anticancer mechanisms of metallodrugs are diverse including DNA damage, protein inhibition, and intracellular reactive oxygen species (ROS) generation [2–5]. Che *et al.* [6,7] reported the gold, platinum, and palladium complexes exhibiting powerful anticancer activity which selectively bind to protein thiols, DNAG-quadruplexes, or mismatched DNA. Recently, a significant breakthrough by Sadler *et al.* [8–12] demonstrated that a series of catalytic ruthenium, osmium and iridium half-

sandwich complexes have been exhibited enhanced anticancer activity towards human cancer cells via transfer hydrogenation between coenzyme NAD⁺ and NADH using non-toxic dose of formate as hydride source (Scheme 1).

Ferroptosis is a non-apoptotic cell death process implicated in many human diseases, especially in cancers, which was recently discovered [13–15]. Mechanistically, ferroptosis is derived from cellular iron accumulation and lipid peroxidation, accompanied by glutathione depletion [15]. It also can be induced by chemical reagents such as erastin, and be suppressed by iron chelators or lipid oxidative-related agents [13,15–18]. Wang *et al.* [18] studied protein carbonylations in ferroptosis process by a quantitative chemo-proteomic method. Jiang *et al.* [14,19] reported that ferroptosis was an autophagic cell death process controlled by cellular iron homeostasis-related proteins. Cellular iron homeostasis and distribution were regulated by specific

†These authors contributed equally to this work.

*Corresponding authors (email: weiwei@nju.edu.cn; jingzhao@nju.edu.cn; zguo@nju.edu.cn)



Scheme 1 Metal-based anticancer complexes (color online).

iron-regulating proteins, e.g. ferritin, ferroportin, transferrin receptor and heme oxygenase [20]. Heme oxygenase 1 (HMOX1) was known to metabolize heme into biliverdin, carbon monoxide, and ferrous iron, and increased HMOX1 activity was shown to increase the cellular iron level and subsequently promoted ferritin production to sequester iron followed with pro-oxidant effects. Reported ferroptosis induction by HMOX1 was mediated by iron augmentation and lipid peroxidation [21–23], and this induction was tightly associated with oxidative stress, due to its predominant sensitivity to oxidative inducers such as redox-active iron, heme, hemoglobin, and heme-containing proteins [24]. Up-regulation of HMOX1 could enhance heme degradation and ferritin synthesis, and change the intracellular iron distribution [25,26]. Thus, the regulation of iron homeostasis and iron-regulated proteins is important to ferroptotic process.

Based on the previous reported Ir(III) anticancer complexes [27,28], we studied a novel mitochondria-targeting Ir(III) complex, IrFN, which could induce ferroptosis in A2780 human ovarian cancer cells. Mechanistic studies by label-free quantitative proteomics profiling were investigated. We also studied iron-dependent cell death, ROS accumulation, lipid peroxidation, and levels of over released iron in A2780 cancer cells. mRNA transcription quantification, *in vitro* over-expression of HMOX1, and RNAi-mediated knock-down experiments were also determined in the present study.

2 Experimental

2.1 Syntheses of nitronyl ligand and IrFN

Nitronyl ligand. Synthesis of nitronyl ligand was referred to

previous reports [29,30]. A solution of isopropyl hydroxylamine hydrochloride (2 mmol, 250 mg), 4-(pyridin-2-yl)-benzaldehyde (2 mmol, 366 mg), Na₂SO₄ (6 mmol, 852 mg), and NaHCO₃ (6 mmol, 504 mg) in dichloromethane (DCM) (15 mL) was refluxed under nitrogen atmosphere for 48 h. The residue was filtered through Celite, and the solvent was then removed on rotary evaporator. The crude product was purified by column chromatography (hexane/ethyl acetate (5:1)), to give a pale yellow solid (yield=446 mg, 93%).

IrFN. The nitronyl ligand (0.55 mmol, 132 mg), IrH₂-(PPh₃)₂(C₃H₆O)₂SbF₆ [27,28] (0.5 mmol, 418 mg) and 3,3-dimethyl-1-butene (2.0 mmol, 257 μL) in acetone (3 mL) were placed in a Schlenk tube, and heated under reflux for 24 h. The solvent was removed under vacuum, and the residue was washed with diethyl ether (20 mL×3). The crude product was then recrystallized from diethyl ether to obtain a pale yellow solid powder (yield=411 mg, 81%).

2.2 Cytotoxicity and cell viability assay

The cytotoxicity of IrFN towards human ovarian cancer cells (A2780), human lung cancer cells (H1299), human normal hepatic cells (L-02), human cervical cancer cells (HeLa), human liver cancer cells (HepG-2), human breast cancer cells (MCF-7), human lung cancer cells (A549), and human fibrosarcoma cells (HT-1080) were determined using 3-[4,5-dimethylthiazol-2-yl]-2,5 diphenyl tetrazolium bromide (MTT) assay.

Cells were seeded in 96-well tissue culture plates for 24 h and then incubated with different concentrations of complexes for 48 h. Subsequently, 30 μL/well of MTT solution was added and incubated for 4 h. After incubation, the culture medium was removed and replaced with 150 μL/well dimethyl sulfoxide (DMSO). The colour intensity of the medium was measured at 550 nm using a microplate reader (Tecan Infinite M1000 PRO) to calculate the cell viability. Half maximal inhibitory concentration (IC₅₀) value of the drug concentration corresponding to the inhibition rate at 50% was calculated using ORIGINPRO 8 statistical analysis. All experiments were conducted three times to ensure the reproducibility of the results.

2.3 Cellular distribution of IrFN

A2780 cells were incubated with 3 μM complex IrFN for 3 h, then washed three times with phosphate buffer saline (PBS). Cells were collected by centrifugation using the Mitochondria/Nuclei Preparation Kit (KeyGEN BioTECH Co., Ltd., China). The nuclei, mitochondria, and remaining cytoplasm fractions were quantified by inductively coupled plasma mass spectrometry (ICP-MS).

2.4 Proteomic analysis

A2780 cells were treated with 5 μM complex IrFN and 5 μM nitron ligand for 3 h, respectively. And cells treated with 0.02% DMSO were used as control. After cells were collected, one volume of SDT buffer (4% sodium dodecyl sulfate (SDS), 100 mM dithiothreitol (DTT), 150 mM Tris-HCl pH 8.0) was added, and the solution was boiled for 15 min and centrifuged at 14,000 g for 20 min. Protein digestion (200 μg for each sample) was performed according to the FASP procedure described by Mann *et al.* [31]. Briefly, the detergent, DTT and other low-molecular-weight components were removed by using 200 μL of UA buffer (8 M urea, 150 mM Tris-HCl, pH 8.0) for repeated ultrafiltration (Microcon units, 30 kD) facilitated by centrifugation. One hundred microlitres of iodoacetamide (0.05 M in UA buffer) was added to block reduced cysteine residues, and the samples were incubated for 20 min in the dark. The filter was washed with 100 μL of UA buffer three times, and with 100 μL of NH_4HCO_3 (25 mM) twice. Finally, the protein suspension was digested with 3 μg of trypsin (Promega, USA) in 40 μL of 25 mM NH_4HCO_3 overnight at 37 $^\circ\text{C}$, and the resulting peptides were collected as a filtrate. The peptide content was estimated by the UV light spectral density at 280 nm by using an extinction coefficient of 1.1 for 0.1% (g/L) solution, calculated based on the frequency of tryptophan and tyrosine in vertebrate proteins. Each fraction was injected into a Q Exactive mass spectrometer (Thermo Scientific, USA) for LC (liquid chromatography)-MS/MS analysis. The detection method was a positive ion, and the ion scanning range was 300–1,800 m/z . The primary mass spectrometer resolution was 70,000 at 200 m/z and the AGC (automatic gain control) target was 1×10^6 , the Maximum IT was 50 ms, and the dynamic exclusion time was 60 s. The mass/charge ratio of the polypeptide and polypeptide fragments was collected as follows: 20 fragments were acquired after each full scan, the MS2 Activation Type was HCD, and the Isolation window was 2 m/z . The rate was 17,500 at 200 m/z , Normalized Collision Energy 30 eV, and Underfill was 0.1%. All identified proteins were retrieved from the UniProtKB human database (Release 2017_02) in FASTA format. In this study, we used the label-free quantification algorithm for quantification [32]. The GO analysis was carried out with Blast2GO. KEGG pathway annotation on the target protein set was performed with KAAS (KEGG automatic annotation server) software. Protein clustering was performed as follows: the quantitative information of the target protein collection was normalized, and then the cluster 3.0 software was used to classify the two dimensions of sample and protein expression, and finally the hierarchical clustering heat map was generated using Java Treeview software. All experiments were repeated three times to ensure the reproducibility of the results.

2.5 Measurement of cellular ROS and lipid peroxidation

Cellular ROS were detected using a Reactive Oxygen Species Assay Kit (KeyGEN BioTECH Co., Ltd., China) following the manufacturer's protocol. Briefly, A2780 cells were seeded onto 6-well plates and treated with 2, 5, and 10 μM solutions of IrFN for 3 h. Cells treated with 0.02% DMSO were used as a control group. Three repetitions were performed for each concentration group. Then cells were washed three times with serum-free Dulbecco's modified eagle medium (DMEM), probed with 10 μM DCFH-DA, and incubated in 5% CO_2 at 37 $^\circ\text{C}$ for 30 min. After washed for three times, cells were collected and fluorescence detection was performed by using the FL-1H channel of a flow cytometer (BD FACSCalibur). The lipid peroxidation level was determined using 5 μM of BODIPY-C11 dye (Invitrogen, USA) by the same approach as above.

2.6 GSH concentration detection

A2780 cells were seeded onto 6-well plates and incubated with 5 and 7.5 μM of IrFN and 5 μM nitron ligand, respectively, for 6 h. Then cells were washed once with PBS and collected by centrifugation, and the supernatant was aspirated. A three-fold volume of the protein removal reagent S solution was added to the cell pellet, and then the samples were subjected to two rapid freeze-thaw cycles using liquid nitrogen and a 37 $^\circ\text{C}$ water bath. Samples were left in the ice bath for 5 min and centrifuged at 10,000 g for 10 min at 4 $^\circ\text{C}$. The supernatant was taken for the determination of total glutathione. GSH detection was performed using Total Glutathione Assay Kit (Beyotime Biotechnology Co., Ltd., China), according to the manufacturer's instructions. The total glutathione content in the treated cells was calculated by comparing the sample to the standard curve.

2.7 Gene expression analysis by quantitative RT-PCR

A2780 cells treated with 5 μM IrFN, 5 μM nitron ligand, 5 μM IrFN with 20 μM deferoxamine (DFO) and 5 μM IrFN with 2 μM Fer-1 were harvested after puromycin selection, and the total RNA was purified using RNA Extraction Kits (OMEGA, USA) according to the manufacturer's instructions. The total RNA was subsequently used in a reverse transcription reaction using the Fastking RT Kit with gDNA (TIANGEN, China). Primers for qPCR were designed with Primer Express. Quantitative PCR was performed on triplicate samples in 96-well format using Power SYBR Green Master Mix (Takara, China) on an Applied Biosystems Cycler set to absolute quantification. The change in expression of a gene between the experimental and control conditions was computed using the $\Delta\Delta t$ method with actin as an internal reference gene.

2.8 *In vitro* over-expression of HMOX1 and RNAi-mediated HMOX1 gene knockdown in A2780 cells

The human cell genome was extracted using a Tissue DNA Kit (OMEGA). The HMOX1 gene fragment was obtained by polymerase chain reaction (PCR) from the cell genome using a eukaryotic expression vector PCI plasmid (Thermo Fisher, USA), and the PCI-HMOX1 plasmid was ligated by restriction enzyme digestion. For over-expression, human A2780 cells were transfected using Lipofectamine 3000 (Invitrogen, USA) following the manufacturer's instructions.

The siRNA of the HMOX1 was designed and synthesized, and si-neg was used as a negative control that does not interfere with any gene. All interference RNAs (siRNAs) were purchased from Genepharma (China). Each siRNA consisted of pools of three to five target-specific 19–25 nucleotides. For siRNA-mediated knockdown, human A2780 cells and HT-1080 cells were transfected using Lipofectamine 3000 (Invitrogen, USA) following the manufacturer's instructions.

2.9 Fluorescent imaging of iron detection

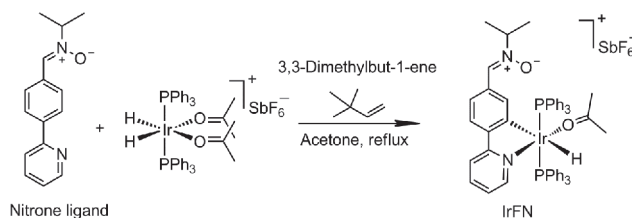
Fluorescent imaging probe FeRhonox-1 (Goryo, Japan) was utilized for the detection of iron in A2780 cells. A2780 cells treated with 5 μM IrFN for 3 h were incubated with 5 μM FeRhonox-1 for 1 h at 37 $^{\circ}\text{C}$, then washed with PBS for three times. Imaging detection was conducted on an Axio Observer Z1 ZEISS fluorescence microscope with Apotome2 software. Iron detection in overexpressed HMOX1 cells and HMOX1 knockdown cells followed the same manufacturer's instruction.

3 Results and discussion

3.1 IrFN is a mitochondria-targeted anticancer metal complex

We first synthesized a new Ir(III) complex IrFN based on the previously reported study (Scheme 2) [27]. Nitronne ligand was synthesized through one-pot reaction of 4-(pyridin-2-yl) benzaldehyde with *N*-isopropyl(*tert*-butyl)-hydroxylamine hydrochloride. The synthesis of the nitronne ligand and complex IrFN was outlined in Scheme 1. A single crystal of complex IrFN suitable for structure determination by X-ray crystallography was obtained via the diffusion method (Figure 1). Besides, IrFN was found to be stable under both physiological condition and biological conditions by high performance liquid chromatography (HPLC) spectrum (Figure S1, Supporting Information online).

Then the cytotoxicity of IrFN and nitronne ligand against human A2780 ovarian cancer cells, H1299 lung cancer cells, L-02 normal hepatic cells, HeLa cervical cancer cells, HepG-2 liver cancer cells, MCF-7 human breast cancer cells, A549



Scheme 2 Synthetic route of complex IrFN.

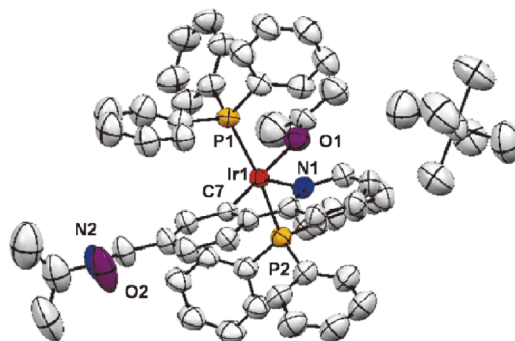


Figure 1 ORTEP diagram for IrFN. Thermal ellipsoids are shown at the 50% probability level. All hydrogen atoms have been omitted for clarity. Bond lengths: Ir(1)–C(7), 2.024(11); Ir(1)–N(1), 2.148(11); Ir(1)–O(1), 2.157(10); Ir(1)–P(1), 2.328(3); Ir(1)–P(2), 2.343(3); bond angles: C(7)–Ir(1)–N(1), 78.0(4); C(7)–Ir(1)–O(1), 172.6(4); N(1)–Ir(1)–O(1), 95.9(4) (color online).

lung cancer cells, and HT-1080 fibrosarcoma cells was determined by the MTT assay using clinical drug cisplatin as a comparison. IrFN was found to have the highest toxicity toward A2780 human ovarian cancer cells with IC_{50} value of 0.69 μM , ca. 25-fold lower than that of cisplatin (17.08 μM , Figure 2(b) and Table S2, Supporting Information online). The cellular uptake of IrFN in A2780 cells was studied by ICP-MS, which was shown approximately 87% accumulation in mitochondria, and it was increased with time (Figure 2(c, d)). These results indicated that mitochondria were the major target of IrFN in cancer cells.

3.2 Label-free quantitative proteomics profiling identified ferroptosis as the target pathway

To further explore the mechanism of action of IrFN in A2780 cells, the label-free quantitative proteomics profiling experiments were performed. As a result, 47 proteins were found significant difference in IrFN treated cells compared with non-treated cells (Figure 3(a)). By comparing with the Kyoto Encyclopedia of Genes and Genomes (KEGG) pathway database, we observed that ferroptosis was the most possible pathway in IrFN treated cells (Figure 3(b)). In this pathway, HMOX1, ferritin light chain (FTL) and MAP1LC3B were found as the most distinct proteins. Furthermore, we performed a label-free quantification analysis

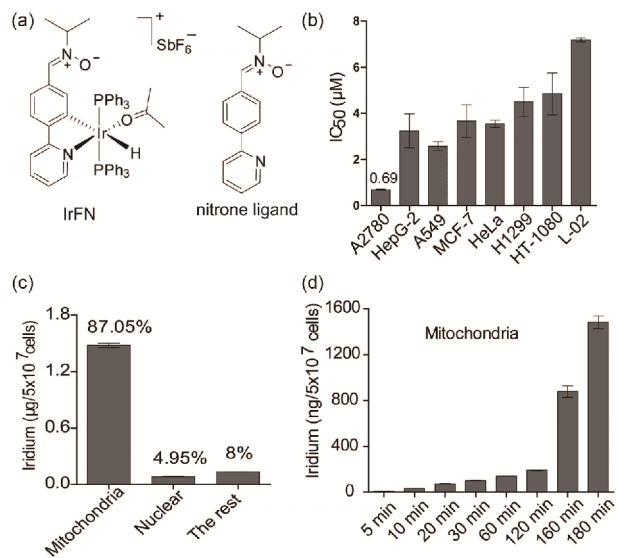


Figure 2 Complex IrFN as a mitochondria-targeting anticancer agent. (a) Chemical structures of IrFN complex and nitron ligand. (b) IC₅₀ values of IrFN towards seven types of cancer cells and one healthy cells L-02. Values are expressed as the mean±SD of triplicates. (c) Cellular distribution of iridium in A2780 cells after 3 h incubation by quantitative ICP-MS. Values are expressed as the mean±SD of triplicates. (d) The content of iridium in mitochondria increased with time. Values are expressed as the mean±SD of two replicates.

in the expression of these proteins. The results of cells treated with 5 μM IrFN showed that the expression level of HMOX1 was increased about 9.8-fold, and the related cellular iron homeostasis proteins, including FTL, MAP1LC3B, ATG5, and NCOA4 were also increased [33] (Figure 3(c)). The increased expression of HMOX1, NCOA4, FTL, and LC3 were further confirmed by Western blot (Figure 3(d)). The expression of the proteins by Western blot was also calculated by integrated density assay (Figure 3(e)). Based on previous reports, activation of HMOX1 increased ferritin (FTL) expression, and the enhanced FTL can bind to ferrous iron and reduce its pro-oxidant effect. The iron-binding ability of ferritin is disturbed by oxidative stress, causing an uncontrolled release of iron, leading to an excessive accumulation of iron and enhancement of lipid peroxidation [25,26]. Combining the above-mentioned distinct proteins, we speculated that IrFN might induce ferroptosis by activating HMOX1. As a control, none of ferroptosis-related proteins was found by the quantitative proteomic screening of the nitron ligand (Figure S4 and Table S5). Notably, most anticancer metallodrugs are known to exert their anticancer activity by inducing apoptosis [34–38], while as far as we are concerned, few reports on metallodrugs causing ferroptosis, especially for iridium complexes, have been revealed.

Next, we first confirmed the IrFN induced cell death via a non-apoptotic form by flow cytometry (Figure S2(a)). Then the ferroptotic cell death was confirmed by treating A2780 cells with IrFN, the determination of cell viability revealed a

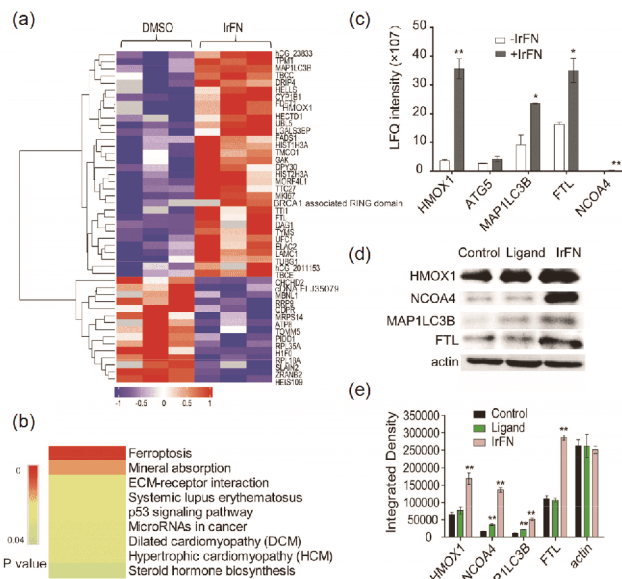


Figure 3 Ferroptosis identification by label-free quantitative proteomics. (a) Heat maps of the 47 distinct proteins detected by label-free quantitative analysis (* $p < 0.05$). (b) KEGG pathway database screens for clear pathways. Statistical significance was assessed using Student's *t*-test. (c) Label-free quantification analysis of the expression of six proteins in cells treated with 5 μM IrFN. (d) Expression of HMOX1, NCOA4, FTL and LC3 in IrFN-treated A2780 cells, compared with the expression in nitron ligand and DMSO-treated control cells by Western blot. (e) Calculated grey-scale of each bands on Western blot membranes. Values are expressed as the mean±SD of triplicate results. Statistical significance was assessed using Student's *t*-test. * $p < 0.05$, ** $p < 0.01$ (color online).

significant suppression in IrFN treated cells compared with controls, while cell inhibition was restored after addition of the iron chelator deferoxamine (DFO). By contrast, the addition of exogenous iron, such as ferric ammonium citrate (FAC), accelerated the cell death caused by IrFN beyond what was observed in DMSO-controls. As an inhibitor of ferroptosis, ferrostatins-1 (Fer-1) was utilized to further identify the IrFN-induced ferroptosis, and cell growth was not significantly inhibited (Figure 4(a) and Figure S2(b)); as a comparison, the nitron ligand displayed no obvious iron-dependent cell viability decrease (Figure S2(c)). Cellular ROS production was measured by H₂DCFDA staining assay and was found to increase about 33 times in IrFN treated cells (Figure 4(b)). The production of ROS was increased with time in 3 h (Figure S3). As a hallmark of ferroptosis, lipid peroxidation was measured in A2780 cells using a lipid peroxidation-sensitive dye BODIPY 581/591 C11[16]. The higher fluorescence intensity by IrFN displayed an increased lipid peroxidation in IrFN treated cells (Figure 4(c)). Besides, ferroptotic cells are morphologically characterized by small mitochondria, collapsed mitochondrial cristae, and increased mitochondrial membrane density [13]. Transmission electron microscopy (TEM) images of the IrFN-treated A2780 cells displayed shrunken mitochondria, a morphological characterization of ferroptosis (Figure 4(d)). Ferropto-

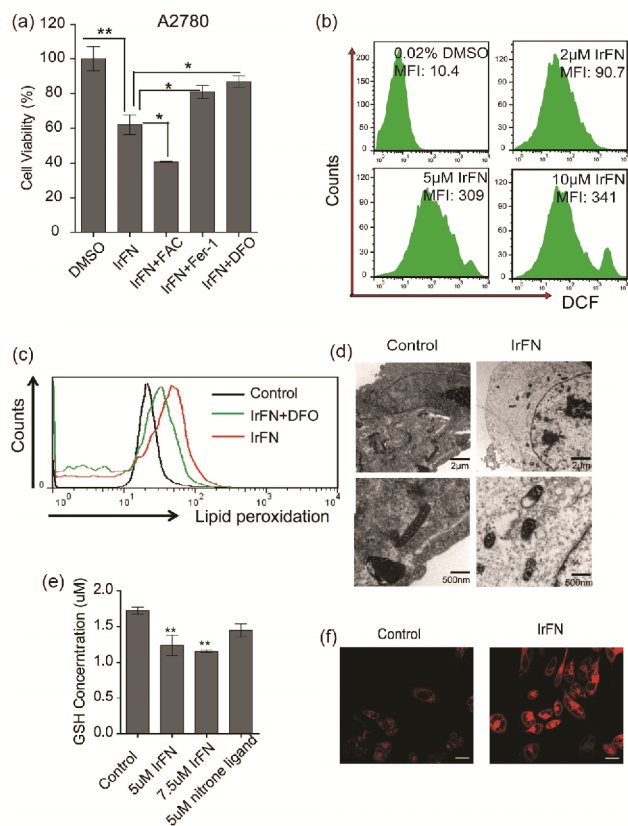


Figure 4 IrFN induced ferroptosis characteristics. (a) Cell viability of A2780 cells treated with 0.02% DMSO, 5 μ M IrFN, 5 μ M IrFN+20 μ M DFO, 5 μ M IrFN+38 μ M FAC, and 5 μ M IrFN+2 μ M Fer-1 for 6 h. (b) ROS production assessed by DCFH-DA staining in 2, 5 and 10 μ M IrFN-treated cells via flow cytometry. (c) Lipid peroxidation production assessed by BODIPY-C11 staining in 0.02% DMSO, 5 μ M IrFN and 5 μ M IrFN+20 μ M DFO treated A2780 cells via flow cytometry. (d) Transmission electron microscopy of A2780 cells treated with 0.02% DMSO and IrFN. (e) GSH concentration in 5 μ M IrFN, 7.5 μ M IrFN and 5 μ M nitronone ligand treated A2780 cells. (f) Fluorescent imaging probe MetalloFluor FeRhox-1 for the detection of iron in 5 μ M IrFN treated A2780 cells. Fluorescence channel: excitation wavelength, 558 nm; emission collected, 575 nm. Scale bar: 20 μ m. Values are expressed as the mean \pm SD of triplicate results. Statistical significance was assessed using Student's *t*-test. * p <0.05, ** p <0.01 (color online).

sis could be triggered during depletion of endogenous inhibitors of ferroptosis, such as the antioxidant and free radical scavenger, tripeptide γ -L-Glu-LCys-Gly (GSH) [15]. By measuring the concentration of GSH, we observed the GSH depletion in IrFN treated cells, leading to the attenuation of antioxidant capacity under high oxidative stress (Figure 4(e)). Besides, over released iron in IrFN treated cells was determined by fluorescent imaging probe (Figure 4(f)); such excessive accumulation of iron, enhancement of ROS, and lipid peroxidation may all contribute to the ferroptotic cell death.

3.3 Ferroptosis in IrFN treated cells by over-expression of HMOX1

Increasing studies have shown that HMOX1 acts as a critical

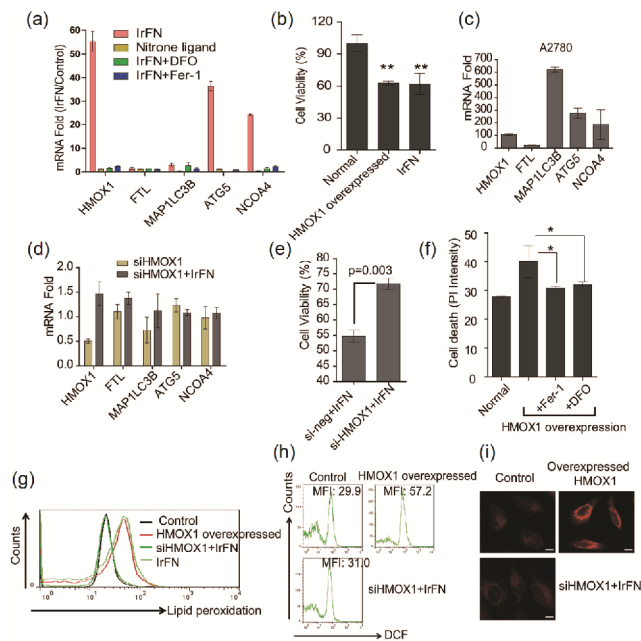


Figure 5 Overexpression of HMOX1 in IrFN induced ferroptosis. (a) mRNA transcription fold change for 5 genes in A2780 cells treated with 5 μ M IrFN, 5 μ M nitronone ligand, 5 μ M IrFN with 20 μ M DFO and 5 μ M IrFN with 2 μ M Fer-1. (b) Comparison of the cell viability of overexpressed HMOX1 in A2780 cells compared with IrFN treated cells. (c) mRNA transcription fold change for six genes in HMOX1 overexpressed cells. (d) mRNA transcription fold change for six genes in siHMOX1 cells and siHMOX1+5 μ M IrFN treated cells. (e) Comparison of the cell viability in siHMOX1 cells and siHMOX1+5 μ M IrFN treated cells. (f) Cell death detection of HMOX1 overexpressed A2780 cells treated with 2 μ M Fer-1 and 20 μ M DFO by PI staining. (g) Production of lipid peroxidation in HMOX1 overexpressed cells, siHMOX1+5 μ M IrFN treated cells and 5 μ M IrFN treated cells via c11-bodipy staining. (h) Production of ROS in HMOX1 over-expressed cells, siHMOX1 cells treated with 5 μ M IrFN, compared with non-treated cells via DCFH-DA staining. (i) Fluorescent imaging probe MetalloFluor FeRhox-1 for the detection of iron in HMOX1 over-expressed and siHMOX1 cells, fluorescence channel: excitation wavelength, 558 nm; emission collected, 575 nm, scale bar: 10 μ m. Values are expressed as the mean \pm SD of triplicate results. Statistical significance was assessed using Student's *t*-test. * p <0.05, ** p <0.01 (color online).

mediator in ferroptosis induction, and plays a causative factor for the progression of several diseases. The critical role of HMOX1 in heme metabolism makes it an important candidate to mediate protective or detrimental effects via ferroptosis induction [21,22,39]. Based on the above proteomic analysis, the expression of HMOX1 in the ferroptosis pathway exhibited the highest level among the other proteins in A2780 cells. The transcription levels of genes in the HMOX1-mediated ferroptosis pathway all increased by using quantitative RT-PCR analysis. In particular, HMOX1 increased by approximately 56-fold in A2780 cells (Figure 5(a)). However, when A2780 cells were treated with nitronone ligand, no obvious change of HMOX1 expression was observed (Figure 5(a)). This result confirmed the high expression of HMOX1 in A2780 cells from mRNA transcription levels. In addition, considering the dependence of the fer-

roptosis process on iron, iron-related control experiments, including the addition of iron chelator and the ferroptosis inhibitor, were also carried out (Figure 5(a)). Two different cell lines, HT-1080, and L-02 normal cells were also treated with IrFN, expression of HMOX1 increased by only 3.6 times in HT-1080, while no significant change in HMOX1 expression was observed in L-02 cells (Figures S5 and S6). These results implied that IrFN could selectively activate HMOX1 in A2780 cells.

To confirm the crucial role of HMOX1 in IrFN induced ferroptosis, a parallel over-expression of HMOX1 by introducing a HMOX1 over-expressed plasmid, and a genetic RNAi-mediated knockdown experiment was performed. The si-neg fragment was designed as the negative control, which did not interfere with any gene in cells. As a result, the downtrends in cell viability after the over-expression of HMOX1 in A2780 cells were similar to the IrFN-induced cell death (Figure 5(b)). Over-expressed HMOX1 promoted the release of iron and over-expression of LC3, FTL, and NCOA4 (Figure 5(c, i)), is consistent with HMOX1 mediated ferroptosis pathway. By contrast, results in siHMOX1 cells showed that the expression of HMOX1 decreased by 50%, indicated that gene knock-down efficiency was ca. 50% (Figure 5(d)). When we treated the siHMOX1 cells with IrFN, limited change of the expression of HMOX1 was observed in A2780 cells (Figure 5(d)). The cell viability results further demonstrated that HMOX1 knockdown suppresses IrFN-induced ferroptotic cell death (Figure 5(e)). Besides, HMOX1 over-expressed cells displayed similar cell death percentage compared with IrFN treated cells (Figure 5(f)). The cell was rescued by addition of ferroptosis inhibitors DFO and Fer-1, which confirmed the ferroptosis pattern involving over-expression of HMOX1 (Figure 5(f)).

Furthermore, enhancement of ROS production, lipid peroxidation, and iron release were also observed in HMOX1 over-expressed A2780 cells after IrFN treatment, but no obvious change found in siHMOX1 A2780 cells (Figure 5(g-i)). Together, all these results suggested that HMOX1 by IrFN activation could promote ROS and lipid peroxidation, and iron accumulation, that induced ferroptosis.

4 Conclusions

In summary, we have described a mitochondria-targeted Ir(III) complex IrFN that induced the iron-dependent ferroptosis in A2780 cells. Label-free quantitative proteomics profiling suggested HMOX1-mediated ferroptosis pathway is the main target pathway of IrFN from KEGG pathway database. An increase of expression of protein HMOX1, autophagic proteins LC3, ferritin FTL, and NCOA4 was observed. Furthermore, dependence of cell death on iron, accumulation of cellular reactive oxygen species, production

of lipid peroxidation, decrease of GSH level and over release of iron induced by IrFN all confirmed the ferroptosis process.

mRNA transcription quantification, overexpression of HMOX1 control and RNAi-mediated knock-down experiment emphasized the role of HMOX1 in IrFN-induced ferroptosis. Over-expressed HMOX1 led to an increase in free iron, accumulation of ROS, and lipid peroxidation. Cell inhibition by HMOX1 over-expression was rescued by adding ferroptosis inhibitors Fer-1 and DFO. Our discovery suggested the first case of anticancer iridium complex, which could induce ferroptosis. Targeting ferroptosis pathways might be a promising approach in the future designs of metallodrugs.

Acknowledgements This work was supported by the National Natural Science Foundation of China (21622103, 21671099, 91753121), Shenzhen Basic Research Program (JCYJ20170413150538897, JCYJ20180508182240106), and the Fundamental Research Funds for the Central Universities (020814380109). F. Chen thanks the International Postdoctoral Exchange Fellowship Program of China. We thank the Shanghai Applied Protein Technology Co., Ltd., for technological assistance.

Conflict of interest The authors declare that they have no conflict of interest.

Supporting information The supporting information is available online at <http://chem.scichina.com> and <http://link.springer.com/journal/11426>. The supporting materials are published as submitted, without typesetting or editing. The responsibility for scientific accuracy and content remains entirely with the authors.

- 1 Rosenberg B, van Camp L, Krigas T. *Nature*, 1965, 205: 698–699
- 2 Jung Y, Lippard SJ. *Chem Rev*, 2007, 107: 1387–1407
- 3 Bruijninckx PCA, Sadler PJ. *Curr Opin Chem Biol*, 2008, 12: 197–206
- 4 Liu Z, Sadler PJ. *Acc Chem Res*, 2014, 47: 1174–1185
- 5 Guo Z, Sadler PJ. *Angew Chem Int Ed*, 1999, 38: 1512–1531
- 6 Zou T, Lok CN, Wan PK, Zhang ZF, Fung SK, Che CM. *Curr Opin Chem Biol*, 2018, 43: 30–36
- 7 Zou T, Lum CT, Lok CN, Zhang JJ, Che CM. *Chem Soc Rev*, 2015, 44: 8786–8801
- 8 Chen F, Soldevila-Barreda JJ, Romero-Canelón I, Coverdale JPC, Song JI, Clarkson GJ, Kasparkova J, Habtemariam A, Brabec V, Wolny JA, Schünemann V, Sadler PJ. *Dalton Trans*, 2018, 47: 7178–7189
- 9 Chen F, Romero-Canelón I, Soldevila-Barreda JJ, Song JI, Coverdale JPC, Clarkson GJ, Kasparkova J, Habtemariam A, Wills M, Brabec V, Sadler PJ. *Organometallics*, 2018, 37: 1555–1566
- 10 Soldevila-Barreda JJ, Romero-Canelón I, Habtemariam A, Sadler PJ. *Nat Commun*, 2015, 6: 6582
- 11 Coverdale JPC, Romero-Canelón I, Sanchez-Cano C, Clarkson GJ, Habtemariam A, Wills M, Sadler PJ. *Nat Chem*, 2018, 10: 347–354
- 12 Liu Z, Romero-Canelón I, Qamar B, Hearn JM, Habtemariam A, Barry NPE, Pizarro AM, Clarkson GJ, Sadler PJ. *Angew Chem Int Ed*, 2014, 53: 3941–3946
- 13 Dixon SJ, Lemberg KM, Lamprecht MR, Skouta R, Zaitsev EM, Gleason CE, Patel DN, Bauer AJ, Cantley AM, Yang WS, Morrison Iii B, Stockwell BR. *Cell*, 2012, 149: 1060–1072
- 14 Gao M, Jiang X. *Curr Opin Cell Biol*, 2018, 51: 58–64
- 15 Stockwell BR, Friedmann Angeli JP, Bayir H, Bush AI, Conrad M, Dixon SJ, Fulda S, Gascón S, Hatzios SK, Kagan VE, Noel K, Jiang

- X, Linkermann A, Murphy ME, Overholtzer M, Oyagi A, Pagnussat GC, Park J, Ran Q, Rosenfeld CS, Salnikow K, Tang D, Torti FM, Torti SV, Toyokuni S, Woerpel KA, Zhang DD. *Cell*, 2017, 171: 273–285
- 16 Yang WS, SriRamaratnam R, Welsch ME, Shimada K, Skouta R, Viswanathan VS, Cheah JH, Clemons PA, Shamji AF, Clish CB, Brown LM, Girotti AW, Cornish VW, Schreiber SL, Stockwell BR. *Cell*, 2014, 156: 317–331
- 17 Dixon SJ, Patel DN, Welsch M, Skouta R, Lee ED, Hayano M, Thomas AG, Gleason CE, Tatonetti NP, Slusher BS, Stockwell BR. *eLife*, 2014, 3: e02523
- 18 Chen Y, Liu Y, Lan T, Qin W, Zhu Y, Qin K, Gao J, Wang H, Hou X, Chen N, Friedmann Angeli JP, Conrad M, Wang C. *J Am Chem Soc*, 2018, 140: 4712–4720
- 19 Gao M, Monian P, Pan Q, Zhang W, Xiang J, Jiang X. *Cell Res*, 2016, 26: 1021–1032
- 20 Cairo G, Recalcati S. *Expert Rev Mol Med*, 2007, 9: 1–13
- 21 Kwon MY, Park E, Lee SJ, Chung SW. *Oncotarget*, 2015, 6: 24393–24403
- 22 Chang LC, Chiang SK, Chen SE, Yu YL, Chou RH, Chang WC. *Cancer Lett*, 2018, 416: 124–137
- 23 Hassannia B, Wiernicki B, Ingold I, Qu F, Van Herck S, Tyurina YY, Bayır H, Abhari BA, Angeli JPF, Choi SM, Meul E, Heyninck K, Declerck K, Chirumamilla CS, Lahtela-Kakkonen M, Van Camp G, Krysko DV, Ekert PG, Fulda S, De Geest BG, Conrad M, Kagan VE, Vanden Berghe W, Vandenabeele P, Vanden Berghe T. *J Clin Investigation*, 2018, 128: 3341–3355
- 24 Clark JE, Foresti R, Green CJ, Motterlini R. *Biochem J*, 2000, 348: 615–619
- 25 Gonzales S, Erario MA, Tomaro ML. *Dev Neurosci*, 2002, 24: 161–168
- 26 Lanceta L, Li C, Choi AM, Eaton JW. *Biochem J*, 2013, 449: 189–194
- 27 Song X, Qian Y, Ben R, Lu X, Zhu HL, Chao H, Zhao J. *J Med Chem*, 2013, 56: 6531–6535
- 28 Wang X, Zhu M, Gao F, Wei W, Qian Y, Liu HK, Zhao J. *J Inorg Biochem*, 2018, 180: 179–185
- 29 Chang ZY, Coates RM. *J Org Chem*, 1990, 55: 3464–3474
- 30 Stoll AH, Blakey SB. *Chem Sci*, 2011, 2: 112–116
- 31 Wiśniewski JR, Zougman A, Nagaraj N, Mann M. *Nat Methods*, 2009, 6: 359–362
- 32 Cox J, Hein MY, Luber CA, Paron I, Nagaraj N, Mann M. *Mol Cell Proteomics*, 2014, 13: 2513–2526
- 33 Hou W, Xie Y, Song X, Sun X, Lotze MT, Zeh III HJ, Kang R, Tang D. *Autophagy*, 2016, 12: 1425–1428
- 34 Liu HK, Sadler PJ. *Acc Chem Res*, 2011, 44: 349–359
- 35 Timerbaev AR, Hartinger CG, Aleksenko SS, Keppler BK. *Chem Rev*, 2006, 106: 2224–2248
- 36 Merkel AL, Meggers E, Ocker M. *Expert Opin Inv Drug*, 2012, 21: 425–436
- 37 Hearn JM, Romero-Canelón I, Qamar B, Liu Z, Hands-Portman I, Sadler PJ. *ACS Chem Biol*, 2013, 8: 1335–1343
- 38 Novohradsky V, Zerzankova L, Stepankova J, Kisova A, Kostrhunova H, Liu Z, Sadler PJ, Kasparkova J, Brabec V. *Metallomics*, 2014, 6: 1491–1501
- 39 NaveenKumar SK, SharathBabu BN, Hemshekhar M, Kemparaju K, Girish KS, Mugesh G. *ACS Chem Biol*, 2018, 13: 1996–2002